Precision measurement of atom-dimer interaction in a uniform planar Bose gas

C. Maury, B. Bakkali-Hassani, G. Chauveau, F. Rabec, S. Nascimbene ⬤, J. Dalibard, and J. Beugnon ⬤

Laboratoire Kastler Brossel, Collège de France, CNRS, ENS-PSL University, Sorbonne Université,
11 Place Marcelin Berthelot, 75005 Paris, France

Cold quantum gases, when acted upon by electromagnetic fields, can give rise to samples where isolated atoms coexist with dimers or trimers, which raises the question of the interactions between these various constituents. Here we perform microwave photoassociation in a degenerate gas of ^{87}Rb atoms to create weakly bound dimers in their electronic ground level. We determine the complete energy diagram of one hyperfine manifold of the least-bound level, which we accurately reproduce with a simple model. Then, from the density-induced shift of the photoassociation line, we measure the atom-dimer scattering length for two weakly bound states of the molecular potential.

Introduction. Cold atomic gases constitute a unique platform to study many-body phenomena. They offer the possibility to relate macroscopic observables, e.g., the equation of state of the fluid, to microscopic quantities such as two- and three-body interactions, as illustrated by the introduction of the "contact parameter" [1]. More generally, with a suitable control of these few-body interactions, quantum gases can host simultaneously atoms and molecules, opening intriguing connections with quantum chemistry [2–7].

The coexistence of atoms and molecular dimers in a quantum gas raises the question of whether a universal description of their interactions exists. In a spin-1/2 Fermi gas close to the unitary limit, the knowledge of the atom-atom scattering length a is sufficient to predict the scattering length a_{ad} characterizing the interaction between an atom and a weakly bound dimer [3,8–17], as well as a_{dd}, the scattering length for dimer-dimer interaction [18]. In a Bose gas in the vicinity of a scattering resonance, the search for a universal relation between a and a_{ad} is more subtle due to the Efimov effect [19], i.e., the existence of a large number of three-body bound states when a increases, which requires the introduction of the so-called "three-body parameter" [20–24]. Outside a resonance, a is comparable to the range of the potential and the existence of a van der Waals universality relating a_{ad} and a for weakly bound dimers remains an open question [25–27].

Experimentally, most studies of atom-dimer interactions in quantum gases concentrated so far on inelastic scattering [28–38] and atom-exchange reactions [39–42]. Elastic collisions have been studied in a Fermi mixture, in which several partial waves contributed to the scattering process [43] and, more recently, in the context of sympathetic cooling of a molecular gas [44]. In this Letter, we study elastic interactions between atoms and *s*-wave dimers in a rubidium Bose gas. The dimers are prepared either in the least or second-to-least bound vibrational ($n = -1$ and $n = -2$) level using microwave photoassociation. Due to the low temperature of the gas, atom-dimer collisions only occur in the *s*-wave channel, and can be parametrized by the scattering length a_{ad}. We first present our measurement of the full Zeeman diagram of the relevant hyperfine manifold for the least-bound level. This allows us to identify the dimer state which is best suited in terms of weak sensitivity to magnetic perturbations. Then, we present a precise spectroscopic measurement of the scattering length a_{ad}, using a uniform atomic gas to minimize inhomogeneous broadening of the signal.

Experimental methods. We use uniform planar Bose gases of ^{87}Rb atoms at low temperature ($k_B T/h \lesssim 400$ Hz) prepared in the strongly degenerate regime, as described in Ref. [45]. The confinement along the vertical direction z is created by an optical accordion lattice operating at the wavelength $\lambda = 532$ nm. We load the atoms from a three-dimensional (3D) Bose-Einstein condensate around a single node of this optical standing wave in a large lattice spacing configuration (≈ 10 µm) and then compress this gas to a short lattice spacing (≈ 2 µm) so as to reach a quasi-two-dimensional (quasi-2D) regime. The resulting approximate harmonic potential of frequency $\omega_z/2\pi \approx 3.7$ kHz along the vertical direction is strong enough to reach the regime $k_B T$, $\mu_a \ll \hbar\omega_z$, where μ_a is the chemical potential of the gas. This ensures the 2D character of the fluid at the thermodynamic level. However, the thickness of the cloud along z, $\ell_z = \sqrt{\hbar/m\omega_z} \approx 180$ nm, remains much larger than the scattering length $a \approx 5$ nm, so that collisions keep a 3D character [46].

The in-plane confinement is created by shaping the profile of a repulsive optical dipole trap with the same wavelength λ. A digital micromirror device allows us to design arbitrary-shaped box potentials. In this work, we mostly use a disk-shaped box potential of radius 20 µm [Fig. 1(a)]. However, for some specific sequences requiring a mixture of Zeeman sublevels, we use instead an array of microtraps, as shown in
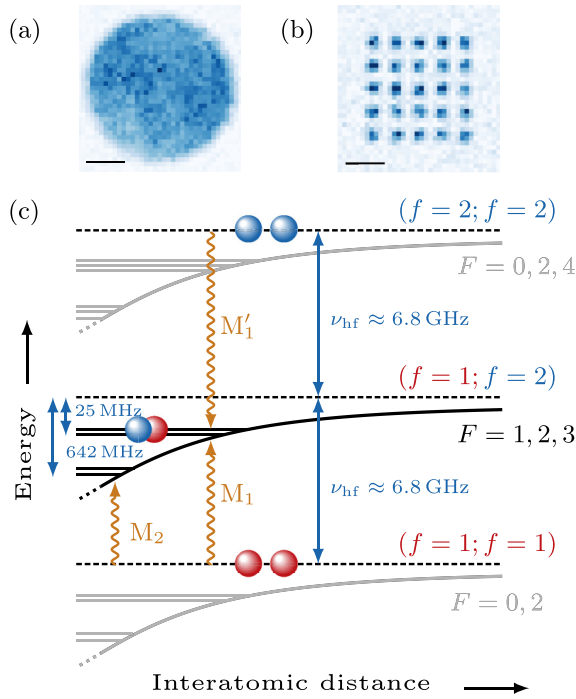
FIG. 1. (a),(b) Clouds used for microwave spectroscopy with either (a) a single component state $|f = 1, m_f = 0, \pm 1\rangle$ or (b) a binary mixture of these hyperfine states (bar length: 10 μm). (c) Relevant levels for a pair of atoms occupying the $f = 1$ or $f = 2$ hyperfine sublevels of the electronic ground state of ^{87}Rb. The dissociation limits of molecular state manifolds, represented as dashed lines, are separated by $h\nu_{\mathrm{hf}} \approx h \times 6.8$ GHz. The molecular potentials are represented by thick continuous lines. The graph is limited to relatively large interatomic distances where van der Waals interaction dominates, hence the superposition of singlet and triplet potentials at the scale of the figure. We also indicate the values of the total spin angular momentum F of the dimer. Here, we focus on the least-bound vibrational levels $n = -1$ and $n = -2$ of the $(f = 1; f = 2)$ subspace, with zero orbital angular momentum. These levels are located ~ 25 and 642 MHz below the dissociation energy, respectively. The dimers are produced by microwave photoassociation of two atoms either both in $f = 1$ (M_1 and M_2 lines) or both in $f = 2$ (M_1' line).
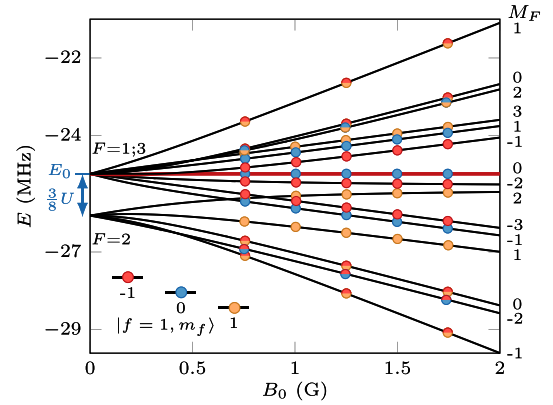

FIG. 2. Energy diagram of the $(f = 1; f = 2)$ subspace. The colors of the experimental points encode the composition of the initial atomic state. The set of solid lines is the result of the simple model described in the text, with two adjustable parameters U and E_0. The state $|\Psi_0^{(n=-1)}\rangle$ used for measuring the atom-dimer scattering length is highlighted with a red solid line. The numbers on the right give, for each state, the quantum number M_F associated with the z component of the spin angular momentum $\hat{F}$.

Fig. 1(b). The 2D density n_a of the cloud is tuned from about 20 to 100 μm^{-2} by removing a controlled fraction of the atoms from the large density configuration [47].

In most experimental sequences, a magnetic field B_0 in the range 0.7–2 G, aligned along the z axis, defines the quantization axis [48]. For photoassociation spectroscopy, we use a microwave field of frequency $\approx$ 6–7 GHz and of amplitude $B_{\mathrm{mw}} \approx 30$ mG, which has nonzero components in all $\pi, \sigma_\pm$ polarizations. We detect the formation of dimers by losses in the gas and we identify for each target state the resonance frequency at which these losses are maximal.

Atomic and molecular levels. For the ^{87}Rb atom, the electronic ground level is split by the hyperfine interaction into two sublevels of spin angular momentum $f = 1$ and $f = 2$. It results from the coupling $\hat{H}_{\mathrm{hf}} \propto \hat{s} \cdot \hat{i}$ between the electron spin $s = 1/2$ and the nuclear spin $i = 3/2$, with $\hat{f} = \hat{s} + \hat{i}$. The two sublevels are separated by an energy difference $h\nu_{\mathrm{hf}} \approx h \times 6.8$ GHz. Atoms can be prepared in any of the

eight states $|f, m_f\rangle$, where m_f is associated to the projection along z of $\hat{f}$. In addition, any binary mixture of these atomic states can be prepared using a series of suitable coherent transfer pulses between these states.

The relevant energy levels for a pair of two atoms labeled A and B are sketched in Fig. 1(c). The unbound states with zero asymptotic kinetic energy are represented as dashed lines. Three subspaces $(f = 1; f = 1)$, $(f = 1; f = 2)$, and $(f = 2; f = 2)$ separated by $h\nu_{\mathrm{hf}}$ can be identified. For each subspace, we indicate the possible values of the total spin (nuclear + electron) angular momentum F (with $\hat{F} = \hat{f}_A + \hat{f}_B$), taking into account the required exchange symmetry for two bosonic atoms. Molecular states corresponding to bound dimers are sketched with solid horizontal lines. We have represented for each subspace the two least-bound vibrational levels $n = -1$ and $n = -2$ with zero orbital angular momentum and binding energies ≈ -25 and -600 MHz, respectively.

Microwave photoassociation spectroscopy. In a first experiment, we photoassociate pairs of atoms in $|f = 1, m_f = 0\rangle \otimes |f = 1, m_f = 0\rangle$ into weakly bound dimers in the $(f = 1, f = 2)$ subspace, on which we now focus. We target the least-bound $(n = -1)$ vibrational level with zero orbital angular momentum and a binding energy $\sim -h \times 25$ MHz [49]. We show in Fig. 2 the measurement of the position of three lines (blue circles) corresponding to the absorption of a photon with a π or $\sigma_\pm$ polarization as a function of the applied external magnetic field B_0. The rest of the diagram is obtained by preparing the initial atomic gas in other pure hyperfine states $|f = 1, m_f = \pm 1\rangle$ or in binary mixtures of $|f = 1, m_f = 0, \pm 1\rangle$. Experiments with mixtures require a modification of the experimental protocol: as the two species have different magnetic moments, residual magnetic field gradients lead to spatial separation of the two components and prevent the dimer formation. We circumvent this problem by

loading atoms in an array of microtraps whose size (about 5 μm) is small enough to prevent phase separation [Fig. 1(b)].

Energy diagram. The energy diagram of Fig. 2 was previously computed using coupled channel calculations [50] and quantum defect theory [51], and it has already been partially measured [52]. We provide below a simple discussion to understand its main features and predict quite accurately the positions of the molecular lines. In all that follows, the dominant term is the hyperfine Hamiltonian $\hat{H}_{\text{hf}} \propto \hat{\boldsymbol{s}}_A \cdot \hat{\boldsymbol{i}}_A + \hat{\boldsymbol{s}}_B \cdot \hat{\boldsymbol{i}}_B$, which gives rise to the three subspaces (f, f') of Fig. 1. The binding energies of the dimer states and the Zeeman shifts are small compared to the splitting $h\nu_{\text{hf}}$ between these subspaces, which allows for a perturbative analysis.

We address first the $B_0 = 0$ case and we consider the total electron spin of the system $\hat{\boldsymbol{S}} = \hat{\boldsymbol{s}}_A + \hat{\boldsymbol{s}}_B$, where $\hat{\boldsymbol{s}}_i$ designates the electron spin operator of atom i. Collisions between two ^{87}Rb atoms involve two channels associated to singlet $S = 0$ and triplet $S = 1$ potentials, with slightly different scattering lengths. The wave functions of the weakly bound dimers are localized at a large interparticle distance, of the order of a few nanometers. At such a distance, van der Waals interactions, which are spin independent and thus identical for the three subspaces (f, f'), dominate and the two potentials are very close to each other. We can thus treat the difference between them by a perturbative approach and model it by the operator

$$\hat{H}_{\text{st}} = U\hat{\boldsymbol{s}}_A \cdot \hat{\boldsymbol{s}}_B = \frac{U}{2}(\hat{\boldsymbol{S}}^2 - 3/2), \tag{1}$$

where the adjustable parameter U is small compared to the binding energy of the dimer and to $h\nu_{\text{hf}}$.

Since $\hat{H}_{\text{st}}$ commutes with $\hat{\boldsymbol{F}}^2$, it only couples states with the same value of F. More precisely, the restriction of $\hat{H}_{\text{st}}$ to the subspace $(f = 1, f = 2)$ splits the $F = 2$ manifold from the $F = 1, 3$ manifolds with the energy shifts $\Delta E_{F=1} = \Delta E_{F=3} = -2\Delta E_{F=2} = U/4$ [53]. Note that due to the large size of a weakly bound dimer, additional magnetic couplings $\propto \hat{\boldsymbol{s}}_A \cdot \hat{\boldsymbol{i}}_B + \hat{\boldsymbol{s}}_B \cdot \hat{\boldsymbol{i}}_A$ play a negligible role [54].

The presence of a magnetic field, described by the Zeeman Hamiltonian $\hat{H}_Z$ (with $\hat{H}_Z \approx 2\mu_B B_0 \hat{S}_z$ if nuclear magnetism is neglected), mixes all F states. However, rotation invariance around the z axis ensures that the projection along z of the spin angular momentum $\hat{\boldsymbol{F}}$ commutes with the Hamiltonian. Since we focus on weakly bound dimers with zero orbital angular momentum, we can label all relevant states by their spin composition and we use the quantum number M_F associated to $\hat{F}_z$ to label the dimer states in Fig. 2.

More quantitatively, the diagonalization of the 36×36 matrix of the spin Hamiltonian $\hat{H}_{\text{hf}} + \hat{H}_{\text{st}} + \hat{H}_Z$ provides the energy shift of the dimer states as a function of magnetic field. It leads, for the least-bound level of the subspace $(f = 1; f = 2)$ studied here, to the 15 continuous lines shown in Fig. 2. These lines are obtained by adjusting two parameters: the coupling [55] U and the energy $E_0 \equiv E_{F=1}(B = 0)$. We find $U = h \times 2.875(5)$ MHz and $E_0 = h \times -24.985(1)$ MHz. This model provides an excellent agreement with all 15 lines in the explored range of magnetic fields. The distance [56] between the best fitted energy diagram and our measurements is 3.7 kHz, which is slightly larger than the uncertainty on the measured molecular line positions ($\lesssim 1$ kHz). The

remaining deviations remind us that the simple model described by Eq. (1) is not exact. A similar study could be performed to measure the Zeeman diagram of weakly bound states in the $(f = 1; f = 1)$ and $(f = 2; f = 2)$ subspaces. However in our case, the lifetime of the atomic sample prepared in $|f = 2\rangle$ is limited by hyperfine changing two-body collisions. It is comparable to the required excitation times which makes these experiments challenging.

The dimer state $|\Psi_0\rangle$. In Fig. 2, we highlighted one particular dimer state, labeled $|\Psi_0^{(n=-1)}\rangle$, and that plays a central role in the following. It is an eigenstate of the restriction of the Hamiltonian $\hat{H}_{\text{hf}} + \hat{H}_{\text{st}} + \hat{H}_Z$ to the $(f = 1, f = 2)$ subspace and its energy is independent of the magnetic field as long as the coupling to the two other subspaces $(f = 1, f = 1)$ and $(f = 2, f = 2)$ induced by $\hat{H}_{\text{st}} + \hat{H}_Z$ can be neglected. Its spin component is $(\sqrt{3}|F = 3, M_F = 0\rangle - \sqrt{2}|F = 1, M_F = 0\rangle)/\sqrt{5}$ and it is a pure electronic spin triplet [53]. When photoassociated from two atoms prepared in a state with a null magnetic moment, it provides us with a "clock" free-bound transition, up to second-order B-dependent shifts $\sim (\mu_B B)^2/(h\nu_{\text{hf}})$.

We have also measured the position of the state with the same spin component in the $n = -2$ level of the same $(f = 1; f = 2)$ subspace. We label it $|\Psi_0^{(n=-2)}\rangle$ and we found the value $h \times -642.219(1)$ MHz for its binding energy at zero magnetic field.

Atom-dimer interaction. We now move to the main result of this Letter regarding the measurement of the elastic interaction between a dimer and the atomic bath from which it is photoassociated. We have studied the interaction of dimers in state $|\Psi_0^{(n)}\rangle$ for $n = -1, -2$ with a bath of atoms in $|f = 1; m_f = 0\rangle$ and the interaction of $|\Psi_0^{(n=-1)}\rangle$ with a bath of atoms in $|f = 2; m_f = 0\rangle$. These three cases correspond to the three microwave association lines, respectively M_1, M_2, and M'_1, shown in Fig. 1(c).

We first detail the study of the M_1 line, associating atom pairs in $|f = 1, m_f = 0\rangle \otimes |f = 1, m_f = 0\rangle$ into the dimer state $|\Psi_0^{(n=-1)}\rangle$. We detect the formation of dimers by losses in the gas as a function of the microwave frequency ν. A typical signal on the M_1 transition is reported in the upper right inset of Fig. 3. The reference frequency ν_0 corresponds to the resonance frequency extrapolated in the zero-density limit [57]. For this reported spectrum, the peak frequency ν_m is displaced with respect to ν_0 by ≈ 670 Hz and the measured full width at half maximum is ≈ 1 kHz. We attribute it to the finite lifetime of the dimers, which can decay through two channels. First, dipolar relaxation within the dimer can produce a pair of atoms by releasing the energy $h\nu_{\text{hf}}$ [58]. Second, two-body inelastic collisions between atoms and molecules can play a significant role, as observed for other alkali molecules [28–30,52].

To study the interaction between the produced dimers and the atom gas, we determine the variation of the peak frequency $\Delta\nu \equiv \nu_m - \nu_0$ with the 2D atomic density n_a. For each density, we adjust the duration of the excitation time to keep the relative depletion at resonance $\delta n_a/n_a$ at a given value. We show the results obtained for three different values of $\delta n_a/n_a$ in Fig. 3. We observe a shift of the resonant frequency which goes up to 800 Hz at our maximum density $n_a \sim$
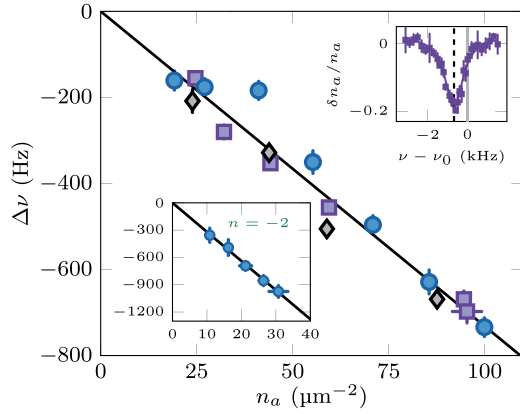
FIG. 3. Frequency shift of the M_1 line as a function of the 2D density of the gas. The three different symbols correspond to a measured relative depletion signal of 20% (square), 14% (diamond), and 8% (circle). All data are adjusted by a common linear fit. The left-hand inset shows the result of a similar measurement for the second-to-least bound level (M_2 line in Fig. 1). The right-hand inset shows a typical microwave photoassociation signal for $n_a = 95\ \mu m^{-2}$. The variation of the width of the photoassociation signal with density is reported in [53].

100 atoms/μm^2. All data collapse on a single curve, which confirms that we operate in the weak excitation regime. We fit a linear function to the data and obtain $\Delta \nu / n_a = -7.3(3)$ Hz/μm^2 [59].

In order to interpret this shift within a mean-field approach, we introduce the interaction parameter $g_{ad} = 2\pi a_{ad} \hbar^2 / m_r$, where $m_r = 2m_a/3$ is the reduced mass of the atom-dimer system. We assume that all interactions occur in the s-wave regime, because of the very low relative momenta between the unbound atoms and the dimer. The photoassociation process must bring to the sample (i) the energy in the zero-density limit $h\nu_0$, (ii) the interaction energy between the dimer and the atom bath, and (iii) the energy $-2\mu_a$, since two atoms are removed from the bath. Denoting $\rho_a(z)$ the 3D density profile of the atom bath and $f_d(z)$ the distribution function of the dimer [with the normalization $\int dz\, \rho_a(z) = n_a$ and $\int dz\, f_d(z) = 1$], we find using the mean-field value of μ_a in the low-temperature limit [53]

$$h\Delta \nu = g_{ad} \int dz\, \rho_a(z) f_d(z) - 2\mu_a = \left(\frac{\sqrt{3}\, a_{ad}}{2a_1} - 2 \right) \mu_a,$$

(2)

where a_f (with $f = 1, 2$) denotes the s-wave scattering length for the collision between two atoms in state $|f, m_f = 0\rangle$. In all cases the dimer density is low enough so that dimer-dimer interactions can be safely neglected.

The atomic 2D density n_a, or equivalently the chemical potential μ_a, are inferred via Ramsey spectroscopy following the method used in Refs. [60,61], which probes the difference of mean-field interaction energies experienced by the atoms in two different internal states. We measure the density-dependent component $\Delta \nu'$ of the microwave frequency that allows a complete transfer, after the two Ramsey pulses, of the gas from the $|f = 1, m_f = 0\rangle$ to the $|f = 2, m_f = 0\rangle$ atomic

state. It reads (see [60,61])

$$h\Delta \nu' = \frac{1}{2} \frac{a_2 - a_1}{a_1} \mu_a$$

(3)

and it depends only on the knowledge of the aforementioned atomic scattering lengths a_f of states $|f, m_f = 0\rangle$. Such a measurement of this frequency shift thus provides a direct calibration of the chemical potential of the gas. Preparing the sample in the same experimental conditions as for the measurement of the frequency shift of the dimer line, we obtain $\Delta \nu'/n_a = -0.52(2)$ Hz/μm^2. Combining Eq. (2) with Eq. (3) we obtain the atom-dimer scattering length:

$$a_{ad} = \frac{4}{\sqrt{3}} a_1 + \frac{1}{\sqrt{3}} \frac{\Delta \nu}{\Delta \nu'} (a_2 - a_1),$$

(4)

an expression which is immune to systematic errors in the calibration of the density n_a. Using the known values of $a_1 = 100.9a_0$ and $a_2 - a_1 = -6a_0$ with a_0 the Bohr radius [62], we obtain

$$a_{ad}^{(n=-1)}[\text{bath in } f = 1] = 184(2)a_0,$$

(5)

where the quoted error takes into account only the uncertainties on $\Delta \nu$ and $\Delta \nu'$ [63]. This value is notably different from the result of the impulse approximation $a_{ad}^{\text{impulse}} = 4(a_1 + a_{12})/3 \approx 261a_0$, where a_{12} is the interspecies scattering length describing the interaction between an $f = 1$ and an $f = 2$ atom. This approximation consists in summing independently the scattering amplitudes of an atom of the bath with each atom of the dimer [64].

Using the M_2 line we have also determined the atom-dimer scattering length of the $|\Psi_0^{(n=-2)}\rangle$ with the same bath. We obtain

$$a_{ad}^{(n=-2)}[\text{bath in } f = 1] = 21(7)a_0$$

(6)

for the atom-dimer scattering length (see inset of Fig. 3). The large difference between $a_{ad}^{(n=-1)}$ and $a_{ad}^{(n=-2)}$ for an identical bath and identical spin states shows the key role of the dimer radial wave function in the scattering process. We note that a related work was performed with two-photon photoassociation of ^{87}Rb atoms for a state in the $n = -2$, ($f = 1; f = 1$) subspace and trapped in a harmonic potential [65]. An atom-dimer scattering length of $-180(150)a_0$ was reported, where the large uncertainty could be attributed to the difficulty of accurately modeling the experimental signal in an inhomogeneous cloud.

Lastly, using the M_1' line we measured the interaction of the dimer state $|\Psi_0^{(n=-1)}\rangle$ with a bath of atoms initially all in state $|f = 2, m_f = 0\rangle$. The fitted slope is now 8.1(9) Hz/μm^2, leading to

$$a_{ad}^{(n=-1)}[\text{bath in } f = 2] = 165(7)a_0,$$

(7)

a value close to the result of an atom bath in state $|f = 1, m_f = 0\rangle$. The similarity between these two results, combined with the small difference between the two bath scattering lengths a_1 and a_2, is compatible with the existence of a "van der Waals universality", which may allow one to link a and a_{ad} for the least-bound dimers.

Conclusions. We have presented a precise measurement of the scattering length a_{ad} characterizing the interaction be-

tween atoms and weakly bound dimers in a degenerate Bose gas. This result provides a first step in the search for a possible van der Waals universality for this problem. Our method can be straightforwardly adapted to other alkali-metal bosonic species. Some of them provide easily accessible Feshbach resonances, making it possible to study the emergence of Efimov physics on a_{ad}. In addition, our precise determination of the whole energy diagram of a weakly bound dimer manifold

paves the way to the implementation of microwave Feshbach resonances [66,67], using for instance strong microwave fields directly generated on atom chips [68].

---

[1] L. Pitaevskii and S. Stringari, *Bose-Einstein Condensation and Superfluidity* (Oxford University Press, New York, 2016), Vol. 164.

[2] L. Viverit, C. J. Pethick, and H. Smith, Zero-temperature phase diagram of binary boson-fermion mixtures, Phys. Rev. A **61**, 053605 (2000).

[3] M. Iskin and C. A. R. Sá de Melo, Fermi-Fermi mixtures in the strong-attraction limit, Phys. Rev. A **77**, 013625 (2008).

[4] C. H. Greene, P. Giannakeas, and J. Pérez-Ríos, Universal few-body physics and cluster formation, Rev. Mod. Phys. **89**, 035006 (2017).

[5] J. L. Bohn, A. M. Rey, and J. Ye, Cold molecules: Progress in quantum engineering of chemistry and quantum matter, Science **357**, 1002 (2017).

[6] L. R. Liu, J. D. Hood, Y. Yu, J. T. Zhang, N. R. Hutzler, T. Rosenband, and K.-K. Ni, Building one molecule from a reservoir of two atoms, Science **360**, 900 (2018).

[7] L. W. Cheuk, L. Anderegg, Y. Bao, S. Burchesky, S. S. Yu, W. Ketterle, K.-K. Ni, and J. M. Doyle, Observation of Collisions between Two Ultracold Ground-State CaF Molecules, Phys. Rev. Lett. **125**, 043401 (2020).

[8] G. V. Skorniakov and K. A. Ter-Martirosian, Three body problem for short range forces. I. Scattering of low energy neutrons by deuterons, Sov. Phys. JETP **4**, 648 (1957).

[9] D. S. Petrov, Three-body problem in Fermi gases with short-range interparticle interaction, Phys. Rev. A **67**, 010703(R) (2003).

[10] C. Mora, R. Egger, A. O. Gogolin, and A. Komnik, Atom-Dimer Scattering for Confined Ultracold Fermion Gases, Phys. Rev. Lett. **93**, 170403 (2004).

[11] J. Levinsen, T. G. Tiecke, J. T. M. Walraven, and D. S. Petrov, Atom-Dimer Scattering and Long-Lived Trimers in Fermionic Mixtures, Phys. Rev. Lett. **103**, 153202 (2009).

[12] F. Alzetto, R. Combescot, and X. Leyronas, Atom-dimer scattering length for fermions with different masses: Analytical study of limiting cases, Phys. Rev. A **82**, 062706 (2010).

[13] M. Iskin, Dimer-atom scattering between two identical fermions and a third particle, Phys. Rev. A **81**, 043634 (2010).

[14] J. Levinsen and D. S. Petrov, Atom-dimer and dimer-dimer scattering in fermionic mixtures near a narrow Feshbach resonance, Eur. Phys. J. D **65**, 67 (2011).

[15] F. Alzetto, R. Combescot, and X. Leyronas, Atom-dimer scattering amplitude for fermionic mixtures with different masses: *s*-wave and *p*-wave contributions, Phys. Rev. A **86**, 062708 (2012).

[16] X. Cui, Atom-dimer scattering and stability of Bose and Fermi mixtures, Phys. Rev. A **90**, 041603(R) (2014).

[17] R. Zhang, W. Zhang, H. Zhai, and P. Zhang, Calibration of the interaction energy between Bose and Fermi superfluids, Phys. Rev. A **90**, 063614 (2014).

[18] D. S. Petrov, C. Salomon, and G. V. Shlyapnikov, Weakly Bound Dimers of Fermionic Atoms, Phys. Rev. Lett. **93**, 090404 (2004).

[19] P. Naidon and S. Endo, Efimov physics: A review, Rep. Prog. Phys. **80**, 056001 (2017).

[20] P. F. Bedaque, H.-W. Hammer, and U. Van Kolck, The three-boson system with short-range interactions, Nucl. Phys. A **646**, 444 (1999).

[21] E. Braaten and H.-W. Hammer, Universality in the three-body problem for ^{4}He atoms, Phys. Rev. A **67**, 042706 (2003).

[22] D. S. Petrov, Three-Boson Problem near a Narrow Feshbach Resonance, Phys. Rev. Lett. **93**, 143201 (2004).

[23] E. Braaten and H.-W. Hammer, Universality in few-body systems with large scattering length, Phys. Rep. **428**, 259 (2006).

[24] C. Gao and P. Zhang, Atom-dimer scattering in a heteronuclear mixture with a finite intraspecies scattering length, Phys. Rev. A **97**, 042701 (2018).

[25] P. Giannakeas and C. H. Greene, Van der Waals universality in homonuclear atom-dimer elastic collisions, Few-Body Syst. **58**, 1 (2017).

[26] P. M. A. Mestrom, J. Wang, C. H. Greene, and J. P. D'Incao, Efimov–van der Waals universality for ultracold atoms with positive scattering lengths, Phys. Rev. A **95**, 032707 (2017).

[27] C. Greene and J. D'Incao (private communication).

[28] P. Staanum, S. D. Kraft, J. Lange, R. Wester, and M. Weidemüller, Experimental Investigation of Ultracold Atom-Molecule Collisions, Phys. Rev. Lett. **96**, 023201 (2006).

[29] N. Zahzam, T. Vogt, M. Mudrich, D. Comparat, and P. Pillet, Atom-Molecule Collisions in an Optically Trapped Gas, Phys. Rev. Lett. **96**, 023202 (2006).

[30] A. Zenesini, B. Huang, M. Berninger, H.-C. Nägerl, F. Ferlaino, and R. Grimm, Resonant atom-dimer collisions in cesium: Testing universality at positive scattering lengths, Phys. Rev. A **90**, 022704 (2014).

[31] T. Lompe, T. B. Ottenstein, F. Serwane, K. Viering, A. N. Wenz, G. Zürn, and S. Jochim, Atom-Dimer Scattering in a Three-Component Fermi Gas, Phys. Rev. Lett. **105**, 103201 (2010).

[32] S. Nakajima, M. Horikoshi, T. Mukaiyama, P. Naidon, and M. Ueda, Nonuniversal Efimov Atom-Dimer Resonances in a Three-Component Mixture of ^{6}Li, Phys. Rev. Lett. **105**, 023201 (2010).

[33] M. T. Hummon, T. V. Tscherbul, J. Kłos, H.-I. Lu, E. Tsikata, W. C. Campbell, A. Dalgarno, and J. M. Doyle, Cold $N + NH$ Collisions in a Magnetic Trap, Phys. Rev. Lett. **106**, 053201 (2011).

[34] R. S. Bloom, M.-G. Hu, T. D. Cumby, and D. S. Jin, Tests of Universal Three-Body Physics in an Ultracold Bose-Fermi Mixture, Phys. Rev. Lett. **111**, 105301 (2013).

[35] K. Kato, Y. Wang, J. Kobayashi, P. S. Julienne, and S. Inouye, Isotopic Shift of Atom-Dimer Efimov Resonances in K-Rb Mixtures: Critical Effect of Multichannel Feshbach Physics, Phys. Rev. Lett. **118**, 163401 (2017).

[36] H. Yang, D.-C. Zhang, L. Liu, Y.-X. Liu, J. Nan, B. Zhao, and J.-W. Pan, Observation of magnetically tunable Feshbach resonances in ultracold ^{23}Na^{40}K $+ ^{40}$K collisions, Science **363**, 261 (2019).

[37] P. D. Gregory, J. A. Blackmore, L. M. Fernley, S. L. Bromley, J. M. Hutson, and S. L. Cornish, Molecule–molecule and atom–molecule collisions with ultracold RbCs molecules, New J. Phys. **23**, 125004 (2021).

[38] S. Jurgilas, A. Chakraborty, C. J. H. Rich, L. Caldwell, H. J. Williams, N. J. Fitch, B. E. Sauer, M. D. Frye, J. M. Hutson, and M. R. Tarbutt, Collisions between Ultracold Molecules and Atoms in a Magnetic Trap, Phys. Rev. Lett. **126**, 153401 (2021).

[39] S. Knoop, F. Ferlaino, M. Berninger, M. Mark, H.-C. Nägerl, R. Grimm, J. P. D'Incao, and B. D. Esry, Magnetically Controlled Exchange Process in an Ultracold Atom-Dimer Mixture, Phys. Rev. Lett. **104**, 053201 (2010).

[40] J. Rui, H. Yang, L. Liu, D.-C. Zhang, Y.-X. Liu, J. Nan, Y.-A. Chen, B. Zhao, and J.-W. Pan, Controlled state-to-state atom-exchange reaction in an ultracold atom–dimer mixture, Nat. Phys. **13**, 699 (2017).

[41] Y.-X. Liu, J. Nan, D.-C. Zhang, L. Liu, H. Yang, J. Rui, B. Zhao, and J.-W. Pan, Observation of a threshold behavior in an ultra-cold endothermic atom-exchange process involving Feshbach molecules, Phys. Rev. A **100**, 032706 (2019).

[42] J. Nan, Y.-X. Liu, D.-C. Zhang, L. Liu, H. Yang, B. Zhao, and J.-W. Pan, Universality in the atom-exchange reaction involving Feshbach molecules, Phys. Rev. A **100**, 062704 (2019).

[43] M. Jag, M. Zaccanti, M. Cetina, R. S. Lous, F. Schreck, R. Grimm, D. S. Petrov, and J. Levinsen, Observation of a Strong Atom-Dimer Attraction in a Mass-Imbalanced Fermi-Fermi Mixture, Phys. Rev. Lett. **112**, 075302 (2014).

[44] H. Son, J. J. Park, W. Ketterle, and A. O. Jamison, Colli-sional cooling of ultracold molecules, Nature (London) **580**, 197 (2020).

[45] J. L. Ville, T. Bienaimé, R. Saint-Jalm, L. Corman, M. Aidelsburger, L. Chomaz, K. Kleinlein, D. Perconte, S. Nascimbène, J. Dalibard, and J. Beugnon, Loading and com-pression of a single two-dimensional Bose gas in an optical accordion, Phys. Rev. A **95**, 013632 (2017).

[46] D. S. Petrov, M. Holzmann, and G. V. Shlyapnikov, Bose-Einstein Condensation in Quasi-2D Trapped Gases, Phys. Rev. Lett. **84**, 2551 (2000).

[47] J. L. Ville, R. Saint-Jalm, É. Le Cerf, M. Aidelsburger, S. Nascimbène, J. Dalibard, and J. Beugnon, Sound Propagation in a Uniform Superfluid Two-Dimensional Bose Gas, Phys. Rev. Lett. **121**, 145301 (2018).

[48] For some molecular transitions of the Zeeman diagram in Fig. 2 the field is oriented in the horizontal plane to maximize the coupling to the molecular state.

[49] R. S. Freeland, Photoassociation spectroscopy of ultracold and Bose-condensed atomic gases, Ph.D. thesis, The University of Texas at Austin, 2001.

[50] T. V. Tscherbul, T. Calarco, I. Lesanovsky, R. V. Krems, A. Dalgarno, and J. Schmiedmayer, rf-field-induced Feshbach res-onances, Phys. Rev. A **81**, 050701(R) (2010).

[51] T. M. Hanna, E. Tiesinga, and P. S. Julienne, Creation and manipulation of Feshbach resonances with radiofrequency radi-ation, New J. Phys. **12**, 083031 (2010).

[52] I. Mordovin, Radio-frequency induced association of molecules in ^{87}Rb, Ph.D. thesis, Swinburne University of Technology, 2015.

[53] See Supplemental Material at http://link.aps.org/supplemental/10.1103/PhysRevResearch.5.L012020 for complementary data and theoretical discussions.

[54] T. Köhler, K. Góral, and P. S. Julienne, Production of cold molecules via magnetically tunable Feshbach resonances, Rev. Mod. Phys. **78**, 1311 (2006).

[55] For simplicity we assume the same value of U for the three subspaces (f, f'). We checked that a 50% change of the value of U for the top or bottom subspaces has no detectable influence on the diagram of the central subspace $(f = 1, f = 2)$.

[56] The distance between the data and the fit is defined as $[\sum_i (\nu_i^{(meas)} - \nu_i^{(fit)})^2 / N_{points}]^{1/2}$, where $\nu_i^{(meas)}$ and $\nu_i^{(fit)}$ are the measured and fitted frequency, respectively, and N_{points} is the number of measured points.

[57] ν_0 differs from ν_{hf} because of the second-order Zeeman effect for the atom and dimer states.

[58] The lifetime of the molecules is much larger than the naive estimate obtained from the known two-body loss rate ($\sim 10^{-14}$ cm^3 s^{-1}) for a pair of atoms in $f = 1$ and $f = 2$ and confined in a volume given by the size of the dimers, i.e., $a^3 \sim 100$ nm^3 (see also [69]).

[59] The data were plotted after subtracting the intercept from the linear fit so that the reference frequency corresponds to the zero-density limit.

[60] Y.-Q. Zou, B. Bakkali-Hassani, C. Maury, É. Le Cerf, S. Nascimbene, J. Dalibard, and J. Beugnon, Magnetic Dipolar Interaction between Hyperfine Clock States in a Planar Alkali Bose Gas, Phys. Rev. Lett. **125**, 233604 (2020).

[61] Y.-Q. Zou, B. Bakkali-Hassani, C. Maury, É. Le Cerf, S. Nascimbene, J. Dalibard, and J. Beugnon, Tan's two-body con-tact across the superfluid transition of a planar Bose gas, Nat. Commun. **12**, 760 (2021).

[62] P. A. Altin, G. McDonald, D. Döring, J. E. Debs, T. H. Barter, J. D. Close, N. P. Robins, S. A. Haine, T. M. Hanna, and R. P. Anderson, Optically trapped atom interferometry using the clock transition of large ^{87}Rb Bose-Einstein condensates, New J. Phys. **13**, 065020 (2011).

[63] The theoretical predictions of [62] for a_f are quoted with no error bars. Previous experiments in our group [60,61] confirmed the prediction for $a_1 - a_2$ with a ~10% accuracy. A shift of $a_1 - a_2$ by this amount would lead to a shift of a_{ad} by a few times the reported uncertainties.

[64] G. F. Chew and G. C. Wick, The impulse approximation, Phys. Rev. **85**, 636 (1952).

[65] R. Wynar, R. S. Freeland, D. J. Han, C. Ryu, and D. J. Heinzen, Molecules in a Bose-Einstein condensate, Science **287**, 1016 (2000).

[66] D. J. Papoular, G. V. Shlyapnikov, and J. Dalibard, Microwave-induced Fano-Feshbach resonances, Phys. Rev. A **81**, 041603(R) (2010).

[67] Y. Ding, J. P. D'Incao, and C. H. Greene, Effective control of cold collisions with radio-frequency fields, Phys. Rev. A **95**, 022709 (2017).

[68] P. Böhi, M. F. Riedel, J. Hoffrogge, J. Reichel, T. W. Hänsch, and P. Treutlein, Coherent manipulation of Bose–Einstein condensates with state-dependent microwave potentials on an atom chip, Nat. Phys. **5**, 592 (2009).

[69] B. J. Verhaar and S. J. J. M. F. Kokkelmans, Stability of rubidium molecules in the lowest triplet state, Phys. Rev. A **95**, 042706 (2017).